JOURNAL OF AIRCRAFT
Vol. 44, No. 6, November–December 2007

Unsteady Numerical Simulation of Wings with Flaperon Flying Over Nonplanar Ground Surface

Jeonghyun Cho,* Jinsoo Cho,† and Seawook Lee‡
Hanyang University, Seoul, 133-791, Republic of Korea

DOI: 10.2514/1.30265

A boundary-element method is developed for the conceptual design of a high-speed transportation system for flying over a nonplanar ground surface. The method is validated by comparing present results with experimental data and other numerical data. Unsteady aerodynamic characteristics of a tandem wing with the flaperon flying over the nonplanar ground surface are investigated using the present method. When a tandem wing with the flaperon flies inside the channel, the lift coefficients of the wings are increased further because the air trapped by the fence of the channel increases the ground effect. On the other hand, the fence of the channel compensates for the lift decrement of the rear wing due to the wake generated by the front wing. Therefore, there is little change between the flat ground and the channel in the longitudinal stability of the wings. Moreover, because the lift increment due to the channel takes place on both sides of the wing with the same rate of increase, there is little difference between the flat ground and the channel in the lateral stability of the wings.

Nomenclature

A, B, C	=	aerodynamic influence matrices
b	=	wing span
c	=	wing chord
d	=	distance between the wing and the fence
h	=	flight altitude of the wing
k, l	=	panel index
N	=	number of panels
n	=	unit normal vector
Q_∞	=	freestream velocity
r	=	magnitude of vector (x, y, z)
S	=	panel area
s	=	distance from the front wing
t	=	time
V_0	=	total kinematic velocity
v_{rel}	=	relative velocity vector of the body-fixed frame
X, Y, Z	=	inertial coordinate
α	=	angle of attack
Δt	=	time step
δ	=	magnitude of deflection
μ	=	doublet strength per unit area
σ	=	source strength per unit area
Φ	=	velocity potential
Ω	=	rotation rate vector of the body-fixed frame
ω	=	reduced frequency

I. Introduction

ENVIRONMENTAL problems have been highlighted all over the world. The enormous amount of energy required by transportation systems throughout the world is a major contributor to global environmental degradation. Development of a substitute transportation system is of vital importance to combat this problem. In recent years, there have been many efforts to develop the new concept vehicles that use the wing-in-ground (WIG) effect as a possible solution [1,2]. Because the study of the WIG effect relating to the takeoff and landing of aircraft was first initiated at the beginning of the 20th century, there has been a wide spectrum of numerical approaches used to calculate the aerodynamic properties of wings in ground effect. Wieselsberger [3] first investigated the WIG effect using the image method. Early studies on the WIG effect were analytic [4,5]. They used conformal mapping to find exact solutions. Goez et al. [6] performed the aerodynamic analysis of a low-aspect-ratio wing-in-ground effect using a PANAIR-panel method developed to predict inviscid subsonic/supersonic flow about an arbitrary configuration. Nuhait and Mook [7] used an unsteady vortex lattice method (VLM) to investigate the unsteady ground effect. Chun and Park [8] showed that water waves have the effect of reducing the lift increase due to the ground effect. Hirata and Kodama [9] used computational fluid dynamics (CFD) to study the ground effect of a three-dimensional wing with end plates. Rozhdestvensky [10] presented mathematical models for the nonlinear aerodynamics of lifting surfaces in extreme ground effect. The rapid increase in computing power makes it possible to use numerical methods in solving the aerodynamic problems of a wing-in-ground effect. Zhang and Zerihan [11] investigated the aerodynamic characteristics of a cambered, double-element, high-lift wing operating in ground effect. They showed that boundary-layer separation and the resultant loss of circulation on the main element cause a sharp reduction in the downforce on a wing with a large flap angle. Han and Cho [12] investigated the wake shapes behind a wing-in-ground effect. Recently, an aerolevitation electric vehicle (AEV) has been proposed as a new concept vehicle that uses the WIG effect [13]. The AEV is an over-the-ground-surface tracked wing-in-ground effect vehicle. This vehicle is propelled by counter-rotating propellers using electricity as a power source. This vehicle must use a high-aspect-ratio wing to provide the sufficient lift force at low-speed flight such as takeoff or landing. However, this high-aspect-ratio wing is unnecessary because the high-aspect-ratio wing increases the weight of the vehicle, and the low-aspect-ratio wing can provide the sufficient lift to levitate the vehicle at high-speed flight. As a result, an alternative transport system named future air-speed transit (FAST) has been proposed. The alternative vehicle is propelled by the linear motor using electricity as a power source and its wing is used for the vehicle stability and control. To develop and design such vehicles, it is necessary to understand the unsteady aerodynamic characteristics of the wing with the control surface flying over the nonplanar ground surface such as the channel. Thus, a boundary-element method based on potential flow theory is developed for the unsteady aerodynamic analysis of the wings flying over the nonplanar ground surface. Unsteady aerodynamic characteristics of the wings with the control surface flying over the

Received 5 February 2007; revision received 17 May 2007; accepted for publication 17 June 2007.

*Graduate Student, School of Mechanical Engineering.
†Professor, School of Mechanical Engineering. Member AIAA.
‡Graduate Student, School of Mechanical Engineering.

nonplanar ground surface are investigated using the present method. The boundary-element method has the advantage that it can solve the three-dimensional flows over the complex bodies with less computing time than other numerical methods. Its use can be extended to nonlinear problems by coupling it with other numerical methods.

II. Numerical Methods

A. Potential-Based Panel Method

The following sections are adapted from [14]. The flow is assumed to be inviscid, incompressible, and irrotational over the entire flowfield, excluding the wing's solid boundaries and its wake. Therefore, a velocity potential $\Phi(X, Y, Z)$ can be defined, and the continuity equation becomes Laplace's equation:

$$\nabla^2\Phi = 0 \tag{1}$$

For a wing moving near the ground surface, it is common to use the image method to consider the ground effect. However, for a wing moving over the ground with a bump or inside the channel, it is difficult to implement the image method directly to the problems investigated. Thus, the domain is extended to the nonplanar ground surface such as the channel.

Consider a body with known boundaries S_B (wing surface), S_W (wake surface), S_G (ground surface), and S_∞ (outer boundary). The wing has the flaperon as the control surface. This wing is divided into two elements hypothetically. One is the main element of the wing. Another is the flaperon element. The flaperon element is deflected when attached to the wing. The general solution to Eq. (1) can be constructed based on Green's identity by the sum of source σ and doublet μ distributions on all of the boundaries:

$$\Phi(x, y, z) = \frac{1}{4\pi}\int_{S_B+S_G+S_W} \mu\boldsymbol{n}\cdot\nabla\left(\frac{1}{r}\right)\mathrm{d}S - \frac{1}{4\pi}\int_{S_B+S_G} \sigma\left(\frac{1}{r}\right)\mathrm{d}S \tag{2}$$

To impose the Dirichlet boundary condition on the surface, the perturbation potential has to be specified everywhere on S_B. If for an enclosed body $\partial\Phi/\partial n = 0$, then the potential inside the body will not change. Thus, Eq. (2) becomes

$$\int_{S_B+S_G+S_W} \mu\boldsymbol{n}\cdot\nabla\left(\frac{1}{r}\right)\mathrm{d}S - \int_{S_B+S_G} \sigma\left(\frac{1}{r}\right)\mathrm{d}S = 0 \tag{3}$$

The basic panel element used in this method has a constant-strength source and/or doublet, and the surface is also planar. The Dirichlet boundary condition on a body will have the following form:

$$\sum_{k=1}^{N} C_k\mu_k + \sum_{l=1}^{N_W} C_l\mu_l + \sum_{k=1}^{N} B_k\sigma_k = 0 \tag{4}$$

in which this condition must hold at any moment t. This equation will be evaluated for each collocation point inside the body and these influence coefficients C_k and C_l of the body and wake doublets, respectively, and B_k of the sources are calculated [14].

B. Unsteady Panel Method

The potential flow solution is included in a time-stepping loop. For cases with fixed geometry the geometrical information, such as panel corner points, collocation points, and normal vectors, must be calculated first. The collocation point is located at the centroid of each quadrilateral panel. Then the time-stepping loop begins and the geometry of the wake panel row adjacent to the trailing edge is established based on the motion kinematics. During each of the following time steps the strength of the latest wake row is computed by using the Kutta condition, and the previously shed wake vortex strengths remain unchanged. Thus, at each time step, for N panels, N equations result in N unknown doublet strengths. If the geometry of the body does not change with time, then the matrix is inverted only once.

The Laplace equation (1) does not directly include time-dependent terms. The time dependency is introduced through the modification of "zero normal flow on a solid surface" and the use of the unsteady Bernoulli equation. The Dirichlet boundary condition for unsteady aerodynamic analysis requires that the source strength be given as follows:

$$\sigma = -\boldsymbol{n}\cdot(\boldsymbol{V}_0 + \boldsymbol{v}_{\mathrm{rel}} + \boldsymbol{\Omega}\times\boldsymbol{r}) \tag{5}$$

The Dirichlet boundary condition when specified at the ith panel's collocation point is influenced by all the N body and N_W wake panels and will have the form

$$\sum_{k=1}^{N} C_{ik}\mu_k + \sum_{l=1}^{N_W} C_{il}\mu_l + \sum_{k=1}^{N} B_{ik}\sigma_k = 0 \tag{6}$$

The strength of all the wake panels is related to the unknown doublet values of the trailing-edge upper and lower panels, via the Kutta condition. Therefore, by resubstituting the trailing-edge condition, we can reduce this boundary condition to include only the body's unknown doublets, and for the first time step it becomes

$$\sum_{k=1}^{N} A_{ik}\mu_k + \sum_{k=1}^{N} B_{ik}\sigma_k = 0 \qquad t = \Delta t \tag{7}$$

where $A_{ik} = C_{ik}$ if no wake is shed from this panel, and $A_{1k} = C_{ik} \pm C_{il}$ if it is shedding a wake panel.

During the subsequent time steps, wake panels will be shed, but their strengths are known from the previous computations. Thus, Eq. (7) is valid only for the first time step, and for $t > \Delta t$ the influence of these N_w wake doublets (excluding the latest row) must be included in the boundary conditions. As a result, Eq. (6) will have the form

$$\sum_{k=1}^{N} A_{ik}\mu_k + \sum_{l=1}^{N_w} C_{il}\mu_l + \sum_{k=1}^{N} B_{ik}\sigma_k = 0 \qquad t > \Delta t \tag{8}$$

The wake is captured as part of the solution with no special treatment. Before advancing to the next time step, the wake rollup procedure is performed. Because the vortex wake is force free, each vortex must move with the local stream velocity. The local velocity is a result of the kinematic motion and the velocity components induced by the wake and the body and is usually measured in the inertial frame of reference X, Y, Z, at each panel's corner point. This velocity can be calculated because the strength of all the singularity elements in the field is known at this point of the calculation. To achieve the wake rollup, at each time step, the induced velocity at each wake panel corner point is calculated in the stationary inertial frame and then the vortex elements are moved by the Euler convection scheme.

III. Results and Discussion

Figure 1 shows the conceptual model of the FAST flying inside the channel. A tandem wing with the control surface is used for vehicle stability and control. To validate the present method for a wing with the control surface, steady results of the present analysis are compared with the experiment results. The lift coefficient and the rolling moment coefficient of a tapered wing with the aileron as the function of angle of attack are shown in Figs. 2 and 3, respectively. The wing has the aspect ratio of 4 and the taper ratio of 0.5. The normalized chord (c_A/c) and the span (b_A/c) of the aileron are 0.1479 and 0.5871, respectively. The magnitude of the aileron deflection increases from 0 to 15 deg. As can be seen in the figure, the present results agree relatively well with experiment data [15] for the low angle of attack.

The calculated lift coefficient and pitching moment coefficient for a NACA0012 wing in pitch oscillation are shown in Figs. 4 and 5, respectively. The comparison with experimental data [14] for pitch oscillation about the airfoil's quarter-chord is obtained by using the large aspect ratio of 1000. The reduced frequency ($\omega c/2Q_\infty$) and the

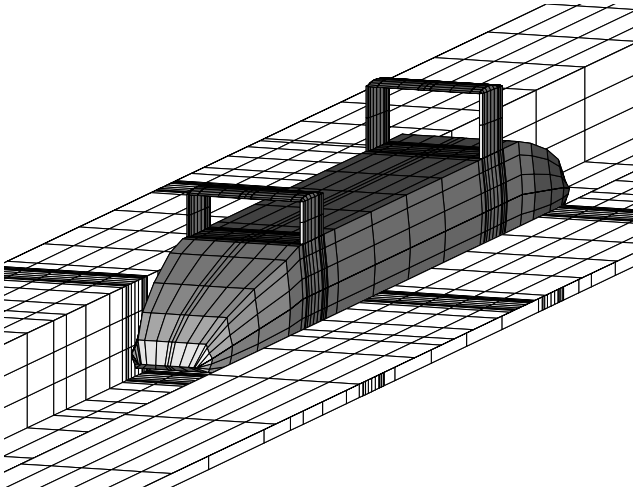

Fig. 1 Conceptual model of the FAST.

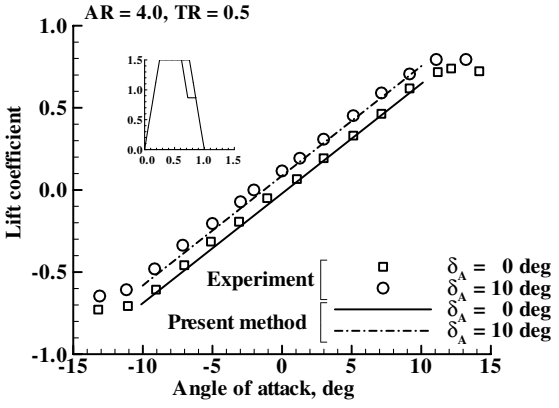

Fig. 2 Lift coefficient for a wing with aileron.

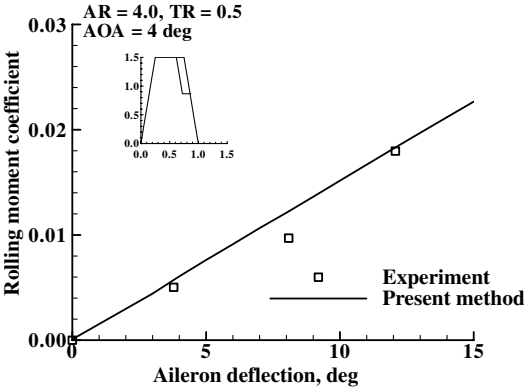

Fig. 3 Rolling moment coefficient for a wing with aileron.

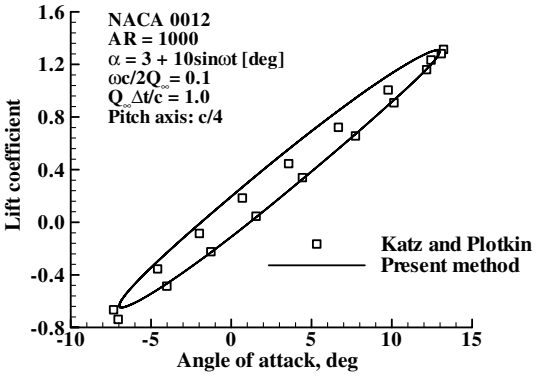

Fig. 4 Lift coefficient for a NACA0012 wing in pitch oscillation motion.

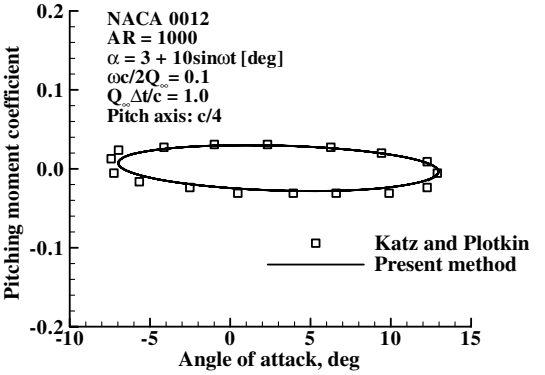

Fig. 5 Pitching moment coefficient for a NACA0012 wing in pitch oscillation motion.

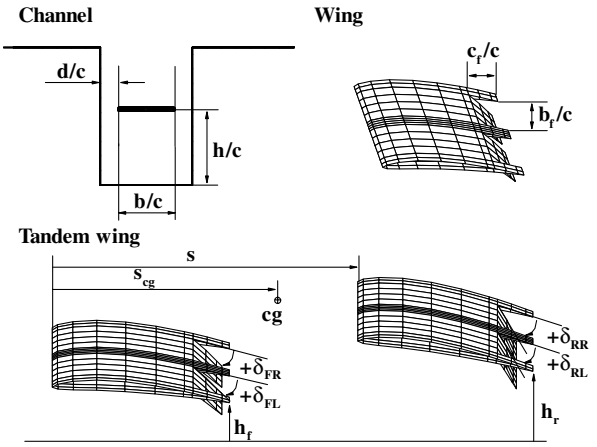

Fig. 6 Nomenclature for a tandem wing system.

time step ($Q_\infty \Delta t/c$) are 0.1 and 1.0, respectively. The present results are reasonably close to the experimental values through the cycle.

The nomenclature for a tandem wing system is shown in Fig. 6. Wake shapes behind a NACA4406 wing in sudden acceleration motion are shown in Fig. 7. The wing has the aspect ratio of 2. The wing is suddenly accelerated with the angle of attack of 2 deg. The time ($Q_\infty t/c$) and the time step ($Q_\infty \Delta t/c$) are 5 and 0.02, respectively. Because the wake is modeled by the constant-strength doublet elements, a starting vortex is shown at the edge of the far-field panel. The wake shape behind the wing out of ground effect is shown in Fig. 7a. Figure 7b shows the wake shape behind the wing-in-ground effect. The wing is suddenly accelerated with the flight altitude of $h/c = 0.2$. It can be seen in the figure that the rolled-up wake for the wing-in-ground effect is diffused compared with the wake for the wing out of ground effect. The wake shape behind the wing-in-ground and fence effect is shown in Fig. 7c. The wing is suddenly accelerated inside the channel. The flight altitude (h/c) of the wing and the distance (d/c) between the wing tip and the fence of the channel are 0.2 and 0.05, respectively. Because the wake diffusion is blocked by the fence of the channel, the wake is on the rise along the fence of the channel. The lift coefficients for the wing flying over the nonplanar ground surface are summarized in Table 1. The nonplanar ground surface increases the lift coefficient. Especially, the channel increases the lift coefficient of the wing further because the wake enclosed by the channel increases the ground effect.

Figure 8 shows the wake shape behind a tandem wing with the flaperon. The distance (s/c) between the front wing and the rear wing

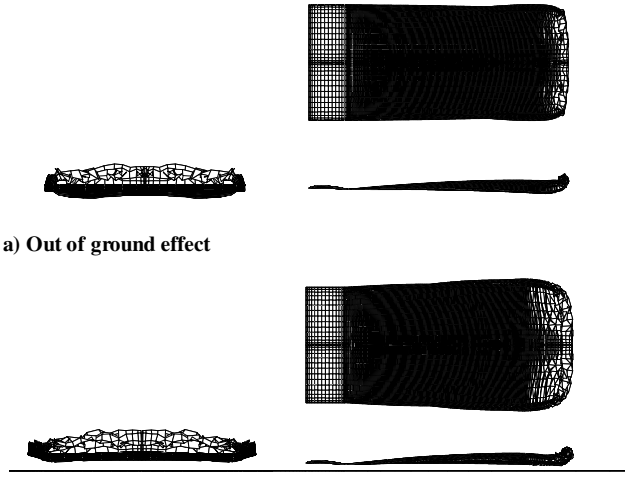

a) Out of ground effect

b) In ground effect

c) In ground and fence effect

Fig. 7 Wake shapes of a wing flying over the nonplanar ground surface.

is 3.0. The flight altitudes of the front wing (h_f/c) and the rear wing (h_r/c) are 0.3 and 1.2, respectively. The center of gravity is in the center of the tandem wing. The normalized chord (c_f/c) and span (b_f/c) of the flap are 0.2 and 0.7, respectively. The time ($Q_\infty t/c$) and the time step ($Q_\infty \Delta t/c$) are 2 and 0.04, respectively. A tandem wing with the flaperon is suddenly accelerated. At $t = 1.2$ the deflection of the left flap is initiated and the flap deflects up to 10 deg at intervals of $\Delta t = 0.4$. Then the tandem wing flies while the flap remains deflected. The aerodynamic coefficients of the wings are shown in Figs. 9–11. The lift coefficients of the wings are increased, following the deflection of the left flap. At $t = 1.6$ the lift coefficients are decreased and then are kept at an even state. The lift coefficient of the front wing is increased due to the deflection of the left flap. On the other hand, the lift coefficient of the rear wing remains the same because the lift increment of the rear wing due to the deflection of the left flap is an offset to the lift decrement due to the wake generated by the front wing. However, on the whole the lift coefficient of the tandem wing is increased due the lift increment of the front wing. The rolling moment is increased also as the left flap deflects. The rolling moment coefficient is suddenly decreased and then is maintained after the deflection of the left flap stopped. However, the total rolling moment of the tandem wing is increased because there is unequal lift distribution due to the deflection of the left flap. The pitching-up moment of the front wing and the pitching-down moment of the rear wing are increased as the left flap deflects. After the left flap ceases deflection, the pitching-up moment coefficient of the front wing is increased, but the pitching-down moment coefficient of the rear wing

Table 1 Lift coefficient for a wing flying over the nonplanar ground surface

Lift coefficient	Unsteady	Steady
Out of ground effect	0.2821	0.2788
In ground effect	0.3796	0.3683
In ground and fence effect	0.4325	0.4141

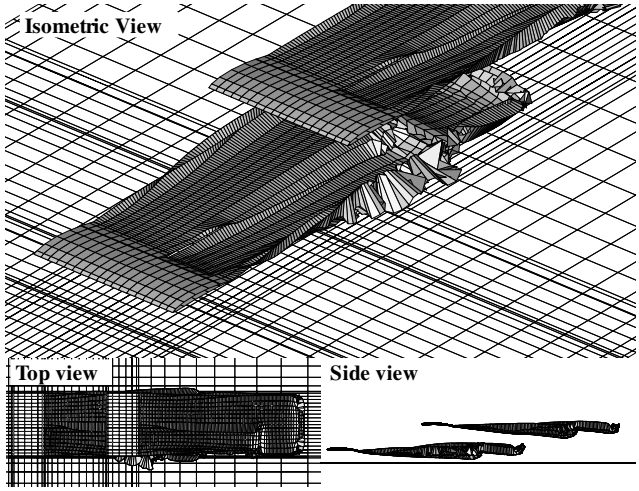

Fig. 8 Wake shape of a tandem wing with the flaperon deflection.

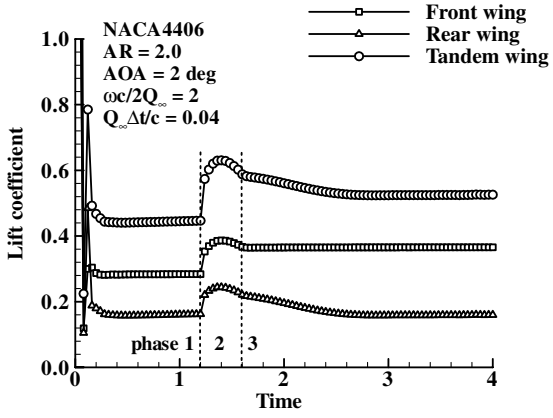

Fig. 9 Transition of the lift coefficient of the wing.

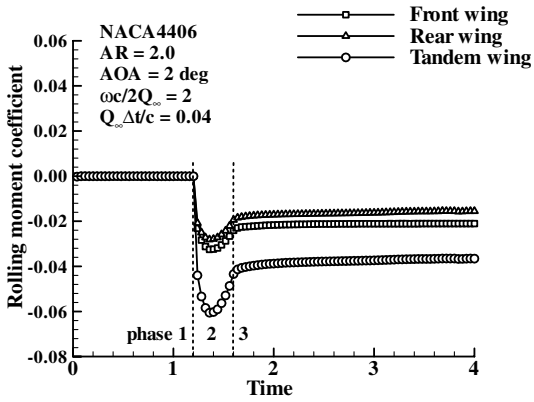

Fig. 10 Transition of the rolling moment coefficient of the wing.

remains the same. This is also due to the wake generated by the front wing causing the lift decrement of the rear wing. However, on the whole the pitching-up moment of a tandem wing is increased due to the lift increment of the front wing.

Figure 12 shows the wake shape behind a tandem wing flying over the flat ground when the one side flap oscillates. The left flap of the wing oscillates with the reduced frequency of $\omega c/2Q_\infty = 2$. The lift coefficients of the wings are shown in Fig. 13. The lift coefficient of the front wing maintains an even loop during the pitch oscillation. On the other hand, the lift coefficient of the rear wing is decreased as the wake generated by the front wing closes to the rear wing. Then the lift coefficient of the rear wing maintains an even loop in the same

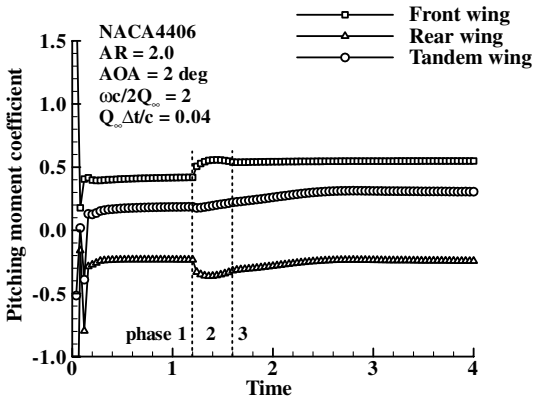

Fig. 11 Transition of the pitching moment coefficient of the wing.

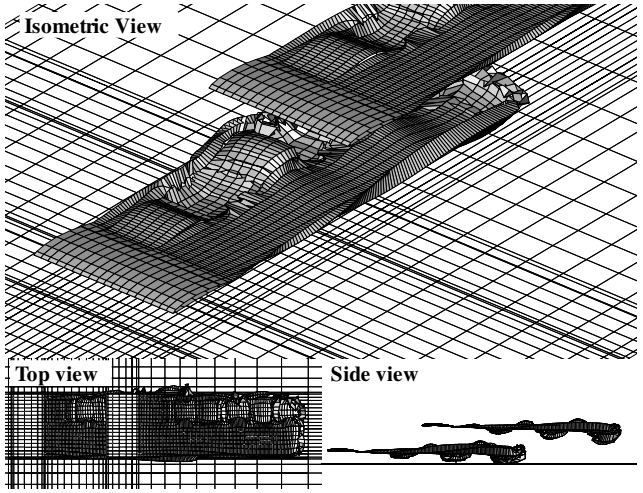

Fig. 12 Wake shape of a tandem wing flying over the flat ground.

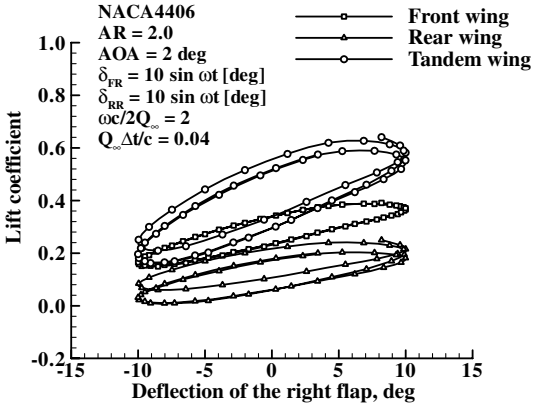

Fig. 13 Lift coefficient of the wing flying over the flat ground.

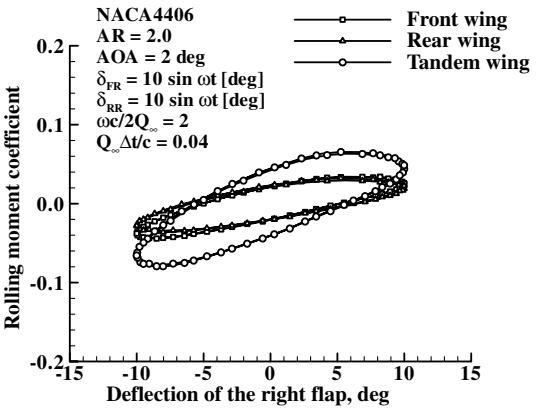

Fig. 14 Rolling moment coefficient of the wing flying over the flat ground.

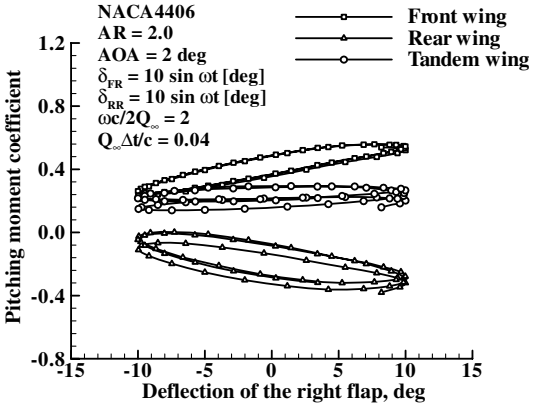

Fig. 15 Pitching moment coefficient of the wing flying over the flat ground.

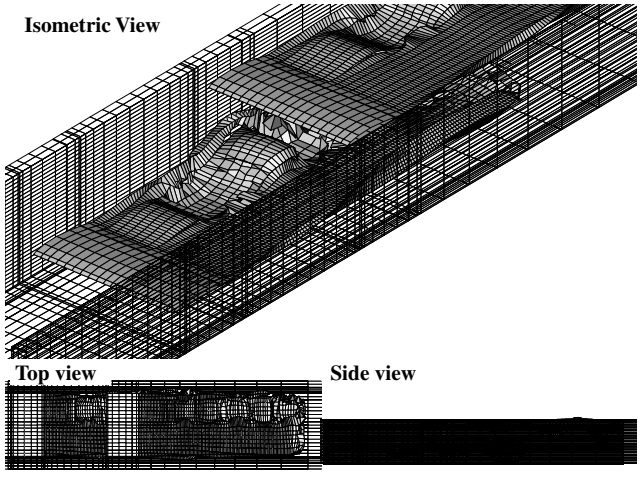

Fig. 16 Wake shape of a tandem wing flying inside the channel.

manner. Figure 14 shows the rolling moment coefficients of the wings. The lift decrement of the rear wing is caused by the wake generated by the front wing with the same rate of decrease. Therefore, there is little difference between the front wing and the rear wing in the rolling moment coefficient. The pitching moment coefficients of the wings are shown in Fig. 15. The pitching-up moment of the front wing maintains an even loop. On the other hand, the pitching-down moment of the rear wing is decreased as the wake generated by the front wing closes to the rear wing. Then the pitching moment coefficient of the rear wing maintains an even loop in the same manner. However, the total pitching-up moment of the tandem wing is increased due to the lift decrement of the rear wing.

Figure 16 shows a wake shape behind a tandem wing flying inside the channel when the one side flap oscillates. The left flap of the wing oscillates with the reduced frequency of $\omega c/2Q_\infty = 2$. The lift coefficients of the wings are shown in Fig. 17. As with the case of the tandem wing flying over the flat ground, the lift coefficient of the tandem wing flying inside the channel maintains an even loop. However, the channel increases the lift coefficients of the wings

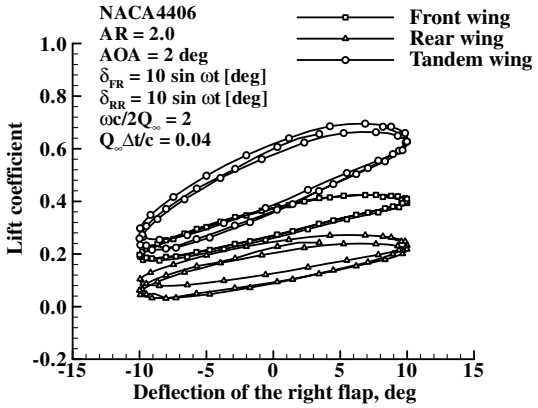

Fig. 17 Lift coefficient of the wing flying inside the channel.

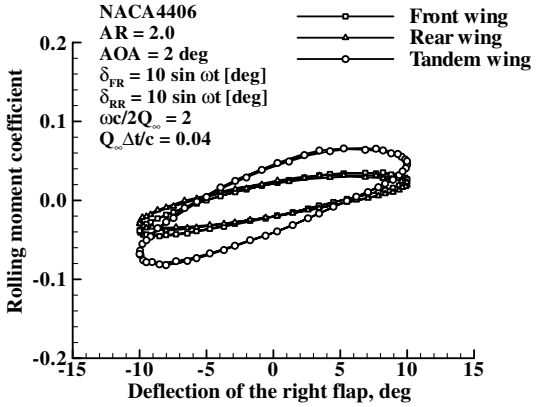

Fig. 18 Rolling moment coefficient of the wing flying inside the channel.

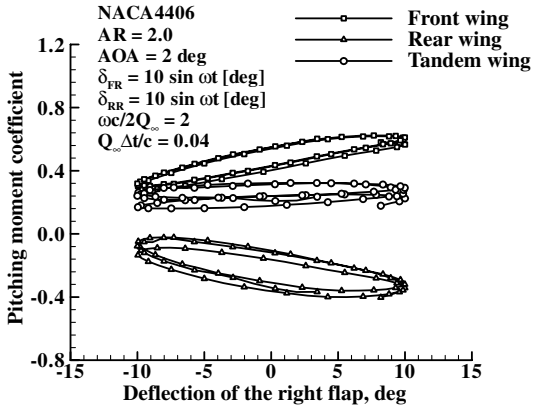

Fig. 19 Pitching moment coefficient of the wing flying inside the channel.

further compared to those of the wings flying over the flat ground. This is due to the trapped air. The air enclosed by the wing, the ground, and the fence increases the ground effect. The rolling moment coefficients of the wings flying inside the channel are shown in Fig. 18. The lift increment due to the channel takes place equally on both sides of the wing with the same rate of increase. Therefore, there is little difference between the wings flying inside the channel and the wings flying over the flat ground in the rolling moment coefficient. The pitching moment coefficients of the wings flying inside the channel are shown in Fig. 19. The pitching-down moment due to the rear wing is increased because the channel compensates for the lift decrement of the rear wing. Therefore, there is no change in the pitching moment of the tandem wing compared to that of the tandem wing flying over the flat ground. In consequence, the channel does not have an influence on the longitudinal stability of the tandem wing.

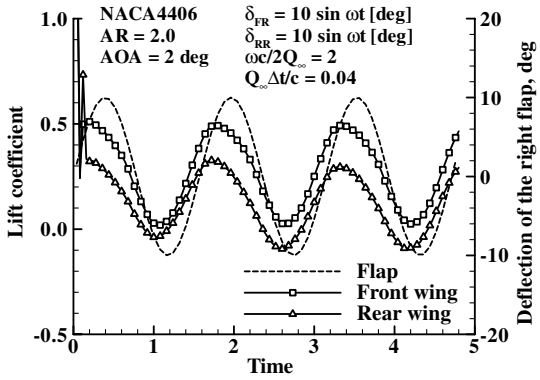

Fig. 20 Phase between the flap deflection and the lift coefficient of the wing.

Figure 20 shows the variation of the flap deflection and the lift coefficients of the wings. The deflection of the flap and the lift coefficients of the wings have an even period. However, the phase difference between the periods is shown in Fig. 20. The phase difference $(Q_\infty t/c)$ is 0.24. This phase difference depends on the reduced frequency of the flap motion and the flight speed of the wing.

IV. Conclusions

Although the present method is limited to the inviscid irrotational assumption, it is believed that the present method will be useful for the conceptual design of the high-speed ground transportation systems flying over the nonplanar ground surfaces. The present method is validated by comparing present results with the experimental and other numerical data. The unsteady numerical simulation of a tandem wing with the flaperon flying over the nonplanar ground surface is performed using the present method. When a tandem wing with the flaperon flies over the nonplanar ground surface, the lift coefficients of the wings are increased. Especially, the nonplanar ground surface such as the channel increases the lift coefficients of the wings further because the air enclosed by the wing, the ground, and the fence of the channel increases the ground effect. At this point, the wake diffusion is obstructed by the fence of the channel, hence the wake is on the rise along the fence of the channel. When a tandem wing with the flaperon flies inside the channel, the fence of the channel compensates for the lift decrement of the rear wing due to the wake generated by the front wing. Therefore, there is little change between the flat ground and the channel in the pitching moment coefficient. Moreover, because the lift increment due to the nonplanar ground surface takes place equally on both sides of the wing, there is little difference between the flat ground and the channel in the rolling moment coefficient. Therefore, it can be deduced that the channel improves the lift performance of the wings, but on the other hand, the channel does not have an influence on the longitudinal stability and the lateral stability of the wings.

Acknowledgment

This work was supported by Grant No. R01-2005-000-10310-0 from the Basic Research Program of the Korea Science and Engineering Foundation.

References

[1] Kono, T., Kohama, Y., and Matsui, N., "Stability of Guide Way Type Wing in Ground Effect Vehicle," *Proceeding of the Third JSME-KSME Fluid Engineering Conference*, JSME, Sendai, Japan, 1994, pp. 715–718.

[2] Kohama, Y., Kikichi, S., Watanabe, H., Ohta, F., and Ito, T., "Evaluation of the Transportation System in Relation to Environmental

Problem," *Workshop on Drag Reduction of Aircraft and Ground Transportation*, Institute of Fluid Science, Sendai, Japan, 2000, pp. 12–13.

[3] Wieselsberger, C., "Wing Resistance Near the Ground," NACA TM-77, April. 1922.

[4] Tomokita, S., Nagamiya, T., and Takenouti, Y., "The Lift on a Flat Plate Near a Plane Wall, with Special Reference to the Effect of Ground upon the Lift of a Monoplane Aerofoil," Aeronautical Research Institute, No. 97, Tokyo, Japan, 1933.

[5] Havelock, T. H., "The Lift and Moment of a Flat Plate in a Stream of Finite Width," *Proceedings of the Royal Society of London, Series A: Mathematical and Physical Sciences*, Vol. 166, No. 925, 1938, pp. 178–196.
doi:10.1098/rspa.1938.0086

[6] Goez, A. R., Osborn, R. F., and Smith, M. L., "Wing-In-Ground Effect Aerodynamic Predictions Using PANAIR," AIAA Paper 84-2495, Oct. 1984.

[7] Nuhait, A. O., and Mook, D. T., "Numerical Simulation of Wings in Steady and Unsteady Ground Effects," *Journal of Aircraft*, Vol. 26, No. 12, 1989, pp. 1081–1089.

[8] Chun, H. H., and Park, I. R., "Analysis of Steady and Unsteady Performance for 3-D Air Wing in the Vicinity of the Free Surface," *Proceedings of a Workshop on Twenty-First Century Flying Ships*, The Institute of Marine Engineers, Sydney, Australia, 1995, pp. 23–46.

[9] Hirata, N., and Kodama, Y., "Flow Computation for Three-Dimensional Wing in Ground Effect Using Multi-Block Technique," *Journal of the Society of Naval Architects of Japan*, Vol. 177, June 1995, pp. 49–57.

[10] Rozhdestvensky, K. V., "Asymptotic and Numerical Methods in the Aerodynamics of the Wings-in-Ground Effect," *Aerodynamics of a Lifting System in Extreme Ground Effect*, 1st ed., Springer–Verlag, Berlin, 2000, pp. 4–22.

[11] Zhang, X., and Zerihan, J., "Aerodynamics of a Double-Element Wing in Ground Effect," *AIAA Journal*, Vol. 41, No. 6, 2003, pp. 1007–1016.

[12] Han, C. H., and Cho, J. S., "Unsteady Trailing Vortex Evolution Behind a Wing in Ground Effect," *Journal of Aircraft*, Vol. 42, No. 2, 2005, pp. 429–434.

[13] Han, C. H., Cho, J. S., Moon, Y. J., Yoon, Y. H., and Song, Y. K., "Design of an Aerolevitation Electric Vehicle for High-Speed Ground Transportation System," *Journal of Aircraft*, Vol. 42, No. 1, 2005, pp. 93–104.

[14] Katz, J., and Plotkin, A., "Unsteady Incompressible Potential Flow," *Low-Speed Aerodynamics*, 2nd ed., Cambridge Univ. Press, Cambridge, England, U.K., 2001, pp. 369–447.

[15] Johnson, B. H., and Demele, F. A., "Investigation of a Thin Wing of Aspect Ratio 4 in the AMES 12 Foot Pressure Wind Tunnel 3—The Effectiveness of a Constant-Chord Aileron," NACA RM-A8I17, Nov. 1948.